NUMERICAL INVESTIGATION OF MOLTEN JET BREAKUP PHENOMENON USING OPENFOAM

THESIS SUBMITTED IN PARTIAL FULFILLMENT OF THE REQUIREMENTS FOR THE DEGREE OF MASTER OF NUCLEAR ENGINEERING

Submitted by:

RITIK KUMAR RAJ

REG. NO: 141069 OF 2017-18

EXAMINATION ROLL NO: M4NUE19006

Under the guidance of

DR. ACHINTYA MUKHOPADHYAY

FACULTY OF MECHANICAL ENGINEERING

JADAVPUR UNIVERSITY, KOLKATA

SCHOOL OF NUCLEAR STUDIES AND APPLICATON

FACULTY OF INTERDISCIPLINARY STUDIES, LAW AND MANAGEMENT

JADAVPUR UNIVERSITY

KOLKATA-700032

MAY 2019

JADAVPUR UNIVERSITY

FACULTY OF INTERDISCIPLINARY STUDIES, LAW AND MANAGEMENT

SCHOOL OF NUCLEAR STUDIES AND APPLICATION

DECLARATION OF ORIGINALITY AND COMPLIANCE OF ACADEMIC ETHICS

It is hereby declared that the thesis entitled "NUMERICAL INVESTIGATION OF MOLTEN JET BREAKUP PHENOMENON USING OPENFOAM" contains literature survey and original research work by the undersigned candidate, as part of his degree of "Master of Nuclear Engineering**"** at the School of Nuclear Studies and Application, Jadavpur University, Kolkata 700032.

All information in this document has been obtained and presented in accordance with academic rules and ethical conduct.

It is also declared that all materials and results, not original to this work have been fully cited and referred throughout this thesis, according to rules of ethical conduct.

Name: RITIK KUMAR RAJ
Registration Number: 141069 of 2017-2018
Examination Roll Number: M4NUE19006
Roll Number: 001730801002
Dated: 28-05-2019

(Signature)
Ritik kumar Raj
Master of Nuclear Engineering
School of Nuclear Studies and Application
Jadavpur University, Kolkata 700032

JADAVPUR UNIVERSITY

FACULTY OF INTERDISCIPLINARY STUDIES, LAW AND MANAGEMENT

SCHOOL OF NUCLEAR STUDIES AND APPLICATION

CERTIFICATE OF RECOMMENDATION

We hereby recommend that this thesis under our supervision by Ritik Kumar Raj, titled "NUMERICAL INVESTIGATION OF MOLTEN JET BREAKUP PHENOMENON USING OPENFOAM", be accepted in partial fulfillment of the requirements for awarding the degree of Master of Nuclear Engineering under Department of Nuclear Engineering of Jadavpur University.

Thesis Guide
Dr. Achintya Mukhopadhyay
Department of Mechanical Engineering
Jadavpur University, Kolkata 700032

Prof. (Dr.) Amitava Gupta
Director
School of Nuclear Studies and Application
Jadavpur University Kolkata 700032

Dr. Pankaj Kumar Roy
Dean
Faculty of Interdisciplinary Studies, Law and Management
Jadavpur University Kolkata 700032

JADAVPUR UNIVERSITY

FACULTY OF INTERDISCIPLINARY STUDIES, LAW AND MANAGEMENT

SCHOOL OF NUCLEAR STUDIES AND APPLICATION

CERTIFICATE OF APPROVAL

The foregoing thesis entitled "NUMERICAL INVESTIGATION OF MOLTEN JET BREAKUP PHENOMENON USING OPENFOAM" is hereby approved as a creditable study of an engineering subject carried out and presented in a satisfactory manner to warrant its acceptance as a prerequisite for the degree of "Master of Nuclear Engineering**"** at the School of Nuclear Studies and Application, Jadavpur University, Kolkata 700032, for which it has been submitted. It is understood that by this approval the undersigned do not necessarily endorse or approve any statement made, opinion expressed or conclusion drawn there in but approve the thesis only for the purpose for which it is submitted.

Committee of the final examination for evaluation of thesis:

---------- ----------

---------- ----------

Signature of Examiners

ACKNOWLEDGEMENT

I would like to express my grandest gratitude to Prof. Achintya Mukhopadhyay for giving me the opportunity to work under his wonderful guidance and also for his encouragement throughout the project work. With his enthusiasm and great efforts to explain things clearly and simply, I could understand the concepts well. He has been considerate while dealing with my mistakes and limitations.

I extend my thanks to all the professors and research scholars of the Neptune Lab in Mechanical Engineering Department of Jadavpur University, especially, Priyankan datta and Aranyak Chakravarty for providing the orientation on the project. It gave a valuable insight on the background and significance of the project. They were the real helpers for me in the absence of the guide. I am grateful to Sachin jain for helping me with OpenFOAM in the initial stage of project and teaching me the codes of MATLAB image processing tools.

I would also like to thanks to my friends for their cooperation and support and also for wonderful time we spent during the course curriculum.

Finally, I am grateful to my parents, for their encouragement and unconditional support during all my academic years.

Date: sign:

ABSTRACT

During a hypothetical severe accident in a nuclear power plant, molten corium could fall in the form of jet into a water pool. The process of jet breakup is very crucial during the fuel-coolant interaction and also, may lead to steam explosion. A numerical study has been established to predict the behavior of Molten Fuel Coolant Interactions.

The present work deals with a study of computational fluid dynamics (CFD) on the melt jet falling into a water pool in order to get qualitative and quantitative understanding of initial premixing phase of FCI. An opensource CFD code OpenFOAM version 6 is used for the 2D numerical analysis employing Volume of Fluid (VOF) method. This work can be divided into three parts; first a verification of earlier work of Thakre et al. which was a modelling of jet fragmentation and estimation of jet breakup length and the effect of jet diameter, jet injection velocity on breakup length. That modelling was done using a commercial CFD code ANSYS FLUENT 14.0, a 2D numerical analysis with VOF method. Second, a study of size distribution of jet droplets and its sphericity using MATLAB R2014b image processing tool. And third, a simulation and breakup pattern in presence of cylindrical channels with in the domain. Which resembles an experimental setup of jet fragmentation done at Jadavpur University and arrangement is more similar to a Pressurised heavy water reactor (PHWR).

NOMENCLATURE

C_o	Courant number
D	jet diameter (mm)
L	jet breakup length (mm)
P	pressure (Pa)
Re	Reynolds number
S	source term
t	time (s)
V, U	relative velocity between droplet and coolant (m/s)
We	Weber number
g	acceleration due to gravity
Greek letters	
α	volume fraction
ρ	coolant density (kg/m^3)
ρ	droplet density (kg/m^3)
λ	wave length (m)
σ	surface tension (N/m)
μ	droplet viscosity (Pa.s)
Subscripts	
a	ambient
c	coolant, critical
d	droplet
j	jet
l	liquid
r	relative
s	surroundings

LIST OF ACRONYMS

BWR	Boiling water reactor
CFD	Computational Fluid Dynamics
CFL	Courant-Friedrichs-Lewy
CSF	Continuous Surface Force
FCI	Fuel-coolant interactions
FOAM	Field Operation and Manipulation
FVM	Finite volume method
JU	Jadavpur University
KHI	Kelvin-Helmholtz Instability
KTH	Kungliga Tekniska Högskolan
MFCI	Molten fuel coolant interaction
PWR	Pressurised water reactor
PHWR	Pressurised heavy water reactor
PISO	Pressure-implicit with splitting of operators
PIMPLE	Combined Pressure-Implicit with Splitting of Operators and Semi-Implicit Method for Pressure Linked Equations
RPV	Reactor pressure vessel
RTI	Rayleigh-Taylor Instability
SIMPLE	Semi-implicit method for pressure-linked equations
VOF	Volume of fluid

LIST OF TABLES

LIST OF FIGURES

CONTENTS

CHAPTER 1

INTRODUCTION

1.1 Theoretical Background

Fuel-coolant interactions (FCI) happens when molten core falls into a water pool. The reactions which occur when the liquid metal comes in contact with the water (cooler volatile liquid), known as FCI or the Molten Fuel-coolant interactions (MFCI). Generally, there are two cases of FCI occurs in a nuclear power plant (NPP) viz. in-vessel case and ex-vessel case. The situation in which, the molten core or part of the molten core comes in contact with coolant of the lower plenum in the form of jets called the in-vessel case. Whereas, when the molten melt or molten metal jet fall into the containment cavity breaching the bottom of reactor pressure vessel (RPV), the situation known as ex-vessel case. When melt jet falls into the water pool fragmentation of water jet starts and simultaneously due to higher degree of superheat or rapid heat transfer vapour generation also starts. The generated vapour insides the water pool surrounds the fragmented particles which lowers the cooling of melt jet.

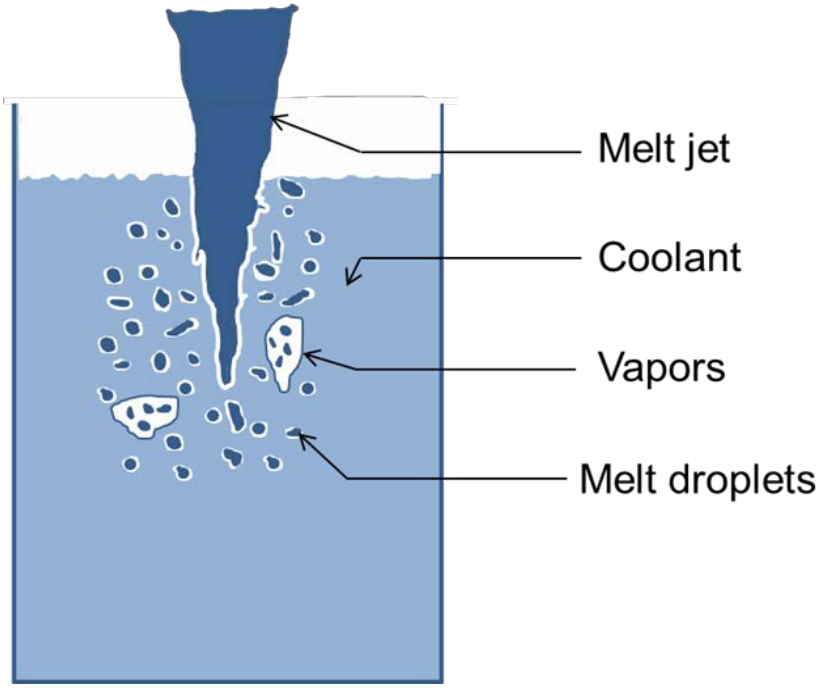

FIG 1. CONCEPTUAL PICTURE OF FCI [1]

In some cases, the energy transfer rate between melt and coolant suddenly become so rapid and coherent that an explosion result. This phenomenon is also known by names of molten fuel-coolant interactions, steam explosions and vapour explosions [2] [3]. Further, in some cases due to the rapid cooling of melt jet, it settles down on the bottom of the reactor vessel. In case of complete fragmentation i.e. melt drops are sufficiently cooled to solidify, the melt will form a bed also called debris bed. the melt progression might stop due to further cooling of the debris bed by the water pool. This stage is known as the premixing of the fuel–coolant interaction [3].

According to the paper of Ryusuke Saitoa et al. [4], the Fukushima Daiichi nuclear power plant (BWR Plant) accident, happened due to melting of core and by falling into the lower plenum of the plant. So, after the Fukushima Daiichi nuclear power plant accident, the importance of an NPP safety measure and study is increasing. Especially, it is important to estimate the condition of the lower plenum of RPV. The structure of lower plenum in case of boiling water reactor (BWR) is more complicated due to the presence of control rod guide tubes and control rod drive housings etc. with respect to pressurized water reactor (PWR). Also, the depth between the reactor core and the RPV lower plenum is more in BWR. When molten core falls into the lower plenum of the BWR, it is supposed that the behaviour of molten material jet would be affected by these complicated structures. So, it is difficult to estimate the behaviour of molten core in the BWR. The jet breakup and fragmentation behaviour are a very critical process of relocation of molten core and cooling of debris at severe accident. Since, the fragmentation phenomenon was complicated by vapour bubble formation, collapse and mixing. For a better understanding of the hydrodynamic instability and fragmentation aspect of the FCI, experiments with molten Wood's metal (melting point 70°C) and water as coolant have been chosen as the model. Thus, we are considering a simplified hydrodynamic case for the modelling and simulation of molten jet and coolant interaction.

1.2 Literature survey

The Molten Fuel-Coolant Interaction shows two important physical phenomena. First are the interfacial instabilities between two fluids due to fluid mechanical interactions and the second is the heat transfer from the superheated melt to coolant resulting in solidification of the melt and vaporization of the coolant to varying degrees.

The instability and breakup of a molten jet stream into droplets has been widely studied starting with the first linear stability analysis of Rayleigh and Taylor [5], to further theoretical developments by Tomotika [6], Meister and Scheele [7], Lee and Flumerfelt [8], Kinoshita [9] and Chacha [10] and experiments by Meister and Scheele [5], Kitamura [11], Saito [12], and others. A comprehensive review was done by Lin & Reitz [13] on the breakup of the isothermal cylindrical jet. Many numerical studies were done with some modelling of the breakup mechanisms. Modelling with the theory of linear instability and traditional CFD models were adopted by many researchers. Reitz [14], Vallet et al. [15] and Ibrahim et al. [16] compiled reviews of these studies. All of these studies investigated the jet breakup behaviour based on the interfacial tension, relative motion, density ratio (ratio of jet and ambient fluid density), jet fluid viscosity and gravity and were limited to isothermal conditions. Hence, none of these studies account for the effect of heat transfer on jet breakup.

As it can be expected, the Molten Fuel Coolant Interactions involve interfacial instabilities in the presence of heat transfer and phase change. The high temperature molten core jet behaviour in the coolant during a severe accident would be largely different from that under isothermal conditions. The simultaneous solidification of melt and, in some cases, vaporization of coolant significantly influences the process. Theofanus and Saito [17] were the first to examine the liquid jet break up with heat transfer and identified the effect of density of coolant phase in jet breakup and mixing. Epstein and Fauske [18] further examined the melt jet breakup including the effect of film boiling. In the thick vapor film case, the vapor (coolant) density was observed to determine the jet breakup whereas in the thin film case liquid coolant density was found to be important. Schins and Gunnerson [19] studied the boiling and fragmentation behaviour of the molten fuel in the liquid sodium experimentally. The fuels used were copper and stainless steel, at initial temperature far above their melting points; and uranium and alumina, initially at their melting points. They found that the transition boiling is the dominating boiling mode for the tested fuels in subcooled sodium. In case of oxide fuel both the fragmentation mechanisms, vapor bubble formation and collapse and thermal stress shrinkage cracking were found to prevail. This was evidenced by the presence of both smooth and fractured particulate. With reference to the paper of Yutaka Abea et al. [20] the formulation behaviour of different fragmentation theories are follows-

1.2.1 Rayleigh–Taylor instability

Rayleigh-Taylor instability is occurred at the head of the jet, due to the jet penetration. In case of displacement of the surrounding fluid the head of jet is resisted by the stagnation pressure due to the surrounding fluid. When the head moving down, the flow velocity of the head is likely to be greater than the velocity of jet, therefore the flow of jet material must have dispersed out in sideways and takes mushroom like shape. This is the earliest theory of jet breakup in which, wavelength at the fastest growth rate is expressed as follows based on the Rayleigh–Taylor instability.

$$\lambda = 2\pi \sqrt{\frac{3\sigma_j}{(\rho_j - \rho_{s)g}}}$$

Using the physical properties of the materials, the relation of the Minimum wavelength and the relative velocity can be calculated.

2.1.2 Critical Weber number Theory

When a droplet exists in a flow, the surface tension balances the shear force from the relative velocity of the fluids. The critical Weber number

$$We_c = \frac{\rho_s U^2 d}{\sigma_j}$$

For the turbulent flow, We_c becomes

$$We_c = 18$$

From these two equations, the most stable droplet diameter in the flow is expressed as

$$d = \frac{18\sigma_j}{\rho_s U^2}$$

Using the physical properties of the materials, the relation of the Minimum wavelength and the relative velocity can be calculated.

2.1.3 Kelvin–Helmholtz instability

At the interface between two parallel streams of liquids Kelvin-Helmholtz instability may occur. This instability occurs due to the difference in flow velocities at interface of deformation. Such type of instability can create oscillations of the jet surface, which may develop and cause tearing of jet material from the jet. This is known as jet atomization. This is the likeliest theory of jet breakup. In the Kelvin–Helmholtz

instability on the interface parallel to the direction of gravity, the critical relative velocity above which some initial disturbances of large wavelength are unstable is given by

$$U = \sqrt{\frac{2\pi\sigma j(\rho_j - \rho_s)}{\lambda\rho_j\rho_s}}$$

Once the relative velocity is obtained, the minimum unstable wavelength is given by

$$\lambda = \frac{2\pi\sigma j(\rho_j - \rho_s)}{U^2\rho_j\rho_s}$$

Using the physical properties of the materials, the relation of the minimum wavelength and the relative velocity can be calculated.

The breakup behaviours (breakup length and transition between regimes) of a molten jet falling in another immiscible fluid are studied and quantified in terms of Weber and Reynold's numbers. Different regimes of jet breakup mentioned in Ginsberg [21] for the various Reynold's number these regimes are laminar, transition, turbulent and atomization. Using the ambient Weber number ($We_a = \frac{\rho_l U^2 D}{\sigma}$) where ρ_l is the density of ambient liquid, U, D and σ are velocity, jet diameter and surface tension respectively Bürger et al. [22] studied the hydrodynamic jet breakup behavior. Also, did a compression of several breakup regimes according to We_aas shown in figure 1.2 (the qualitative behavior is observed with the liquid jet in gas environment).

According to Bürger et al. [22] in case of isothermal breakup or the non-boiling condition as the melt jets are enters the coolant pool, the jet and coolant interface are subject to disturbances and these initial disturbances will grow with time to break the jet. The two major mechanisms responsible for breakup of jet are pinching of thin cylindrical jets at circular curvature due to interfacial tension (Rayleigh Instability) and stripping of small droplets from interface due to relative motion (Kelvin Helmholtz Instability). The analysis of such phenomenon typically involves perturbing the governing equations and linearizing them to predict the stability of a given state. If a state is unstable the linear stability analysis predicts positive growth rates of the perturbation.

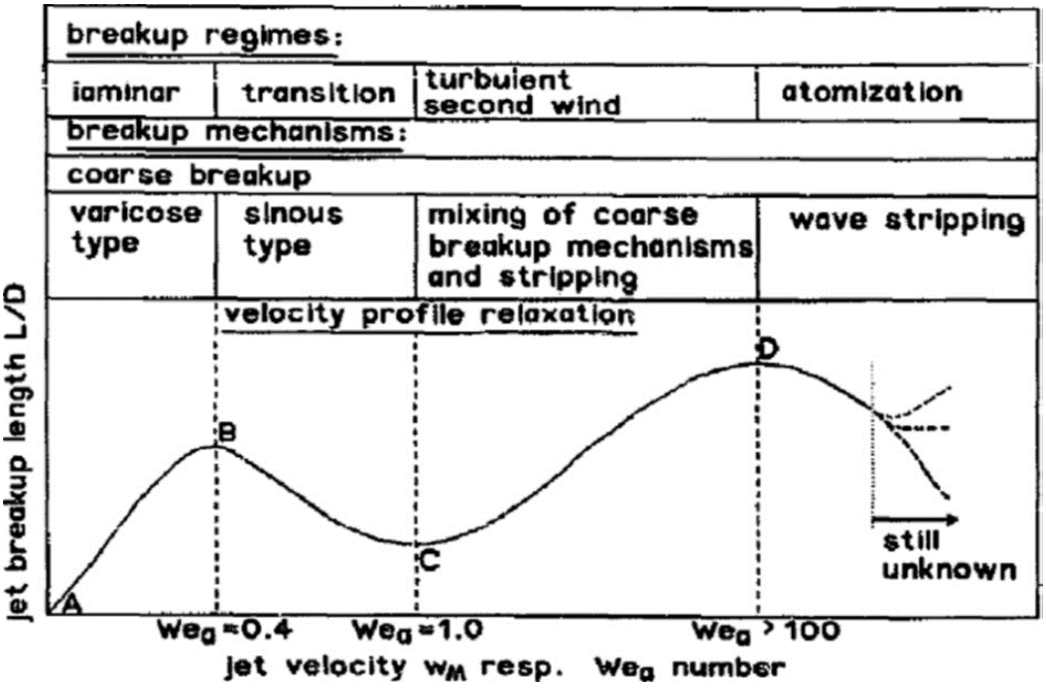

Fig 1.2 Sketch of the jet breakup length curve and related breakup mechanisms [14]

1.3 Present work

The present work aims at improving the melt jet fragmentation/Breakup modelling in order to get a more accurate and reliable prediction of the melt fragmentation as a molten jet is falling into water. Which is motivated from the experimental investigation of melt jet breakup experiments carried out at Jadavpur University in collaboration with Bhabha Atomic Research Centre (BARC). For simplicity, we are considering the interaction between molten metal (taking as a wood's metal) with coolant (water) and a two-dimensional case by assuming that the geometry has a unit length in the z-direction and we are not solving the energy equation instead. The analysis includes the pattern of jet fragmentation which is followed by the study of jet diameter, jet velocity on the jet breakup length and also the size distribution of debris formed. For the numerical simulation purpose, we are using OpenFOAM [23] software (version 6) which is an opensource CFD software. Again, we are try to simulate the jet breakup behaviour in presence of cylindrical channels within the interacting domain.

CHAPTER 2

NUMERICAL METHODOLOGY

As the present modelling is a multiphase non-reacting isothermal and the fluids are (assume as) incompressible, immiscible and Newtonian as well as Stokesian. So, the related solver for the simulations using for the purpose is InterFoam solver [24] [25] which is an incompressible, transient, multiphase, immiscible, isothermal solver and uses the volume of fluid (VOF) method [26] for interface capturing. Also, the InterFoam solver uses the Pressure-Implicit with Splitting of Operators (PISO) algorithm or PISO scheme for pressure-velocity coupling. The following governing equations were solved in finite volume method (FVM) with proper boundary conditions.

2.1 Governing Equations

In the VOF method we solve one momentum equation and one continuity equation. These equations are the same for the two phases. The physical properties of one fluid are calculated as weighted averages based on the volume fraction of the two fluids in one cell. The transport equations for mass, momentum and volume fraction of the phases are summarized as the following -

2.1.1 Continuity Equation:

As the fluid considered here are assumed to be incompressible so the the continuity equation takes the form

$$\nabla \cdot U = 0$$

2.1.2 Momentum Conservation Equation (Navier-Stokes Equation):

$$\frac{\partial \rho U}{\partial t} + \nabla.(\rho UU) - \nabla.\mu\nabla U - \rho g = -\nabla p + F_s$$

Where, F_s is the surface tension force which takes place only at the interfaces. This discontinuous force is very difficult to calculate precisely and some modelling is required to minimize the error. One such model is to calculate it as a function of the volume fraction of a phase.

$$F_s = \sigma k(x) n$$

The solver, interFoam uses VOF method (given by Hirt and Nichols [26]) which captures the interface using a phase fraction (α) approach. In this method, volume fraction is a conserved quantity and is used as a weight to determine the density (ρ) and dynamic viscosity (μ) of the mixture of the two fluids.

$$\rho = \alpha\rho_l + (1-\alpha)\rho_m$$

and, $$\mu = \alpha\mu_l + (1-\alpha)\mu_m$$

2.1.3 Phase-fraction Conservation Equation:

The volume of fluid in a cell is computed as $F_{vol} = \alpha V_{cell}$, where, V_{cell} is the volume of a computational cell and α is the fluid fraction in a cell. The values of α in a cell should range between 1 and 0. At the interface the value of α is between 0 and 1. The scalar function can be computes from a separate transport equation that takes the form:

$$\frac{\partial \alpha}{\partial t} + \nabla.(\alpha U) = 0$$

In OpenFOAM, the necessary compression of the surface is achieved by introducing an extra artificial compression term into the VOF above equation as follow:

$$\frac{\partial \alpha}{\partial t} + \nabla.(\alpha U) + \nabla.(\alpha(1-\alpha)U_r) = 0$$

Where, U_r is a velocity field suitable to compress the interface. This artificial term is active only in the interface region due to the term $\alpha(1-\alpha)$.

For the calculation of surface tension as a continuous volumetric force, the continuous surface force (CSF) model given by Brackbill et al. [27] is used. According to this model, F_s can be approximated as

$$F_s = \sigma k(x) \frac{\rho}{0.5(\rho_l + \rho_m)} n \approx \sigma k(x) n$$

,

where *n* is a unit vector normal to the interface that can be calculated from

$$n = \frac{\nabla \alpha}{|\nabla \alpha|}$$

and κ is the curvature of the interface that can be calculated from

$$\kappa(x) = \nabla . n$$

These equations are implemented in the interFoam solver.

2.2 Finite Volume Schemes:

InterFoam uses PIMPLE algorithm for linking the pressure equation. The finite volume schemes that were chosen for the discretization of the different terms of the governing equations are tabulated below.

Table 2.1

d/dt Schemes	Euler	Divergent Schemes	
Gradient Schemes	Gauss linear	$\vec{\nabla} \cdot (\rho \vec{U} \vec{U})$	Gauss linear Upwind
Laplacian Schemes	Gauss linear coreacted	$\vec{\nabla} \cdot (\vec{U} \alpha)$	Gauss vanLeer
Interpolation Schemes	Linear	$\nabla \cdot (\vec{U} \alpha)$	Gauss linear
Surface Normal Gradient Schemes	Corrected	$\nabla \cdot (\mu(\nabla \cdot \vec{U}))$	Gauss linear

2.3 CFL condition

Courant-Friedrichs-Lewy (CFL) condition or the Courant number (C_o), exhibits a relation between, the transient time-step size, the fluid velocity within the cell and the computational cell size. Which is given as

$$C_o = \frac{\Delta t . v}{\Delta x}$$

where, Δt is the time-step used during the simulations, $. v$ is the fluid velocity and Δx is the size of the computational cell. The maximum value of Courant number should not exceed the value one. A simulation runs for the particular value of C_o and the time

step can be controlled using the CFL condition to stabilize the numerical scheme. $C_o = 0.001$ is used in the present study.

2.4 Image Processing Algorithm

To calculate the fragmented jet droplets size and sphericity, MATLAB 2014b image processing tool codes has been used. The codes implementation path is given below.

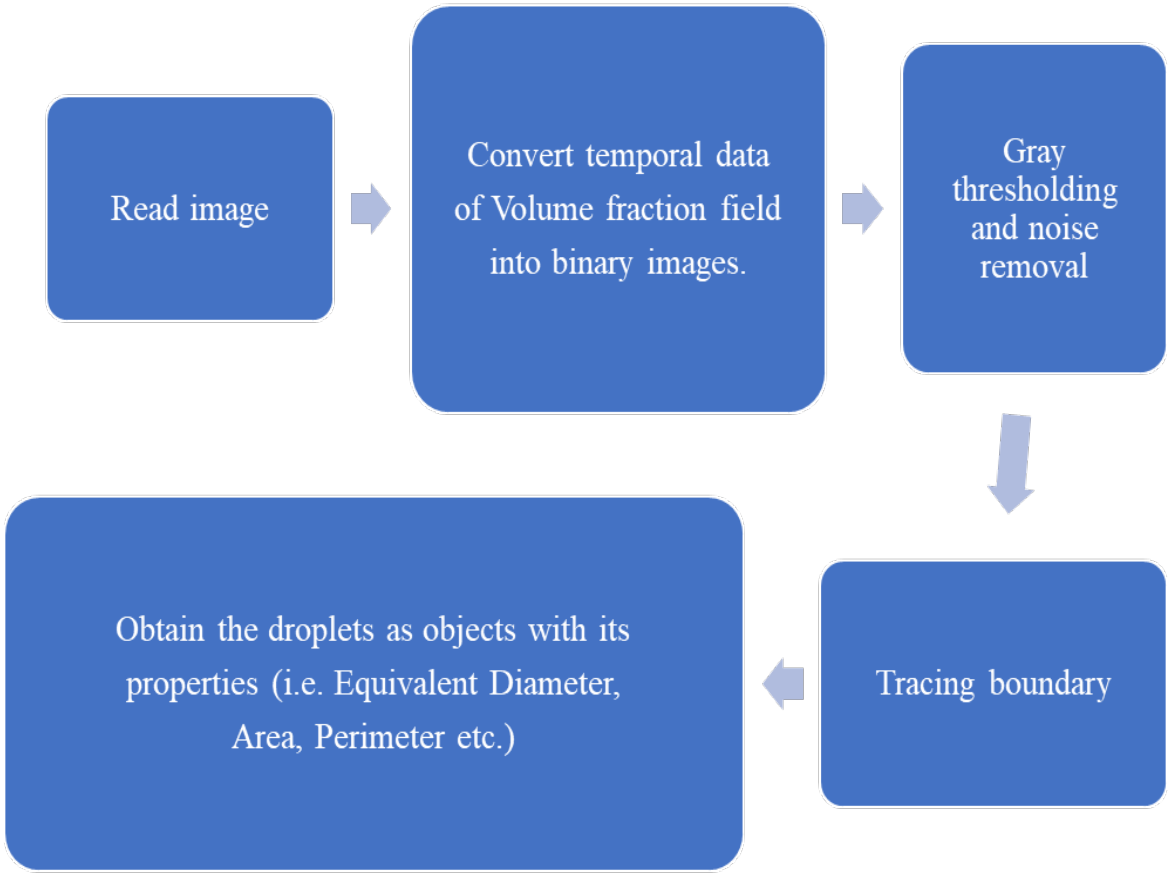

Fig. 2.1 Image processing code implementation path.

CHAPTER 3

RESULTS AND DISCUSSION

3.1 Model validation

The work of Thakre et al. [28], a two-dimensional numerical analysis of melt jet fragmentation which was carried out using a commercial CFD code, ANSYS FLUENT 14.0 is done here with the help of CFD code OpenFOAM 6. The Thakre numerical work was motivated with the experimental investigation of melt jet breakup experiments carried out at Royal Institute of Technology (KTH) Sweden. The two-phase calculation employs volume of fluid method (VOF) where, the phases are treated immiscible. Wood's metal was used as a jet interacting with water, without film boiling. The properties of Wood's metal were taken as

Table 3.1 (in SI units)

Material	Surface tension	Density	Viscosity
Wood's metal	1	9700	0.00194

For the present work, the properties of molten fuel-coolant and method adaptations for solution are taken as same as presented in the paper of Thakre et al. [28], except the mesh adaptation and the software used to run the simulation. The present simulations are carried out using an opensource OpenFOAM software. To simulate the molten jet fragmentation process (huge computational task) a high-performance computing facility PARAM SHAVAK at Jadavpur University have used. The technical specification of the HPC are as follows; It has a processor with dual socket Intel Xeon E5-2670 v3 series with 12 cores each with 2.3GHz Clock speed along with 64 GB ECC DDR4 2133 MHz RAM. There is a NVidia NVS 510 2GB DDR3 graphics accelerator card included in the system with 4 nos. 2TB SATA -3.5" 7200rpm HDD. Developed by C-DAC, India, The PARAM SHAVAK has a peak computing power of 3 teraflops. It takes generally 2 to 5 days run time to simulate each case depending on the jet inlet conditions.

3.1.1 Mesh adaptation:

Accurate capture of the interfaces in two phase flow systems is a bit difficult. for this mesh quality plays an important role. Since, in the paper of Thakre et al. [28], adaptive mesh refinement scheme is used and the optimum mesh dimension taken as $\Delta x = 0.1 \times 0.125$ mm (where Δx represents the finest cell used). But, for validation purpose the mesh quality is assessed by analyzing the results of calculations carried out at various level of mesh refinement at the interfaces and using simpleGrading (a mesh refinement scheme in blockMesh utility) more finer mesh in middle (where $\Delta x = 0.167 \times 0.167$) with respect to sides is used for validation.

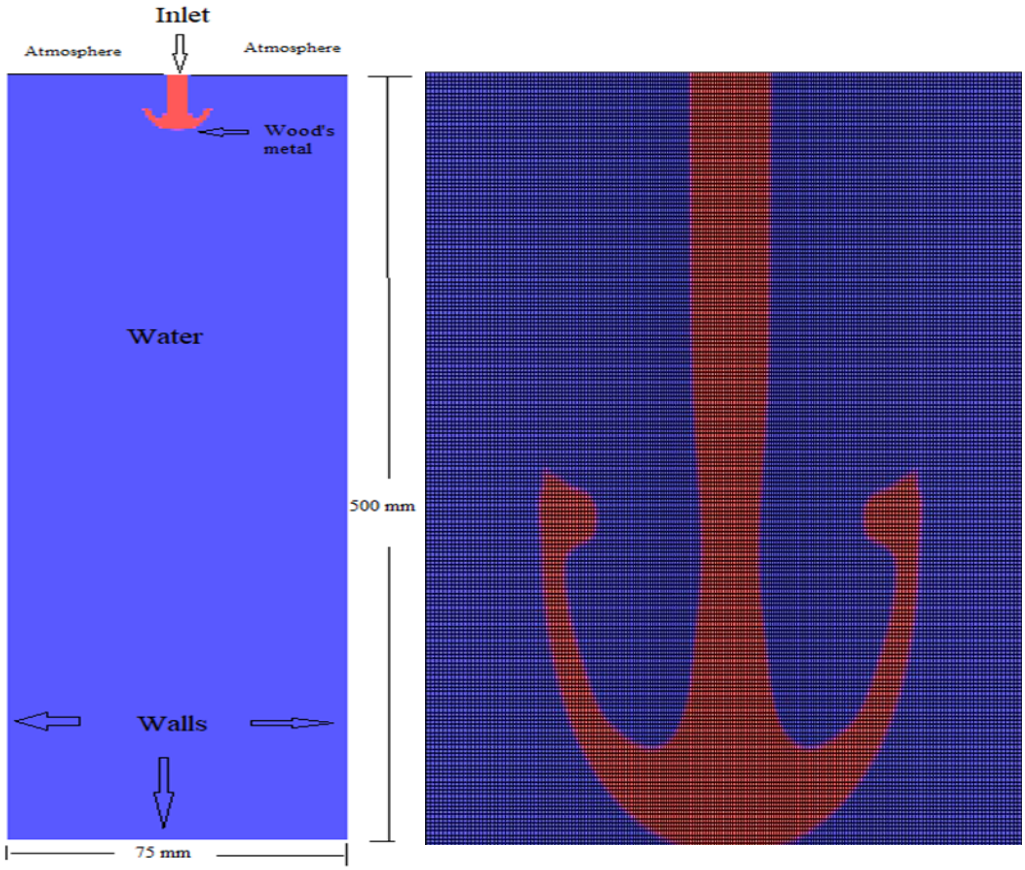

Fig. 3.1 (a) Geometry details and boundary conditions. (b) mesh adaptation

3.1.2 Jet Breakup pattern

The melt jet falling into a coolant may undergo various types of breakup quantitatively depending on the factors such as jet velocity or relative velocity between jet-coolant, and jet diameter. A comparisons of jet breakup between the Thakre et al. [28] paper and the present simulation are shown in figure (3.2) at the different ambient weber number. At lower jet velocities, generally the jet surface tends to remain intact

due to dominance of surface tension effect. However, the jet deforms at the leading edge due to deceleration forces (as shown in Figure 3.2 (I)) and starts stripping in the form of ligaments which further breaks into droplets (it may be treated as a coarse breakup). At some jet velocities, the leading edge deforms into a mushroom-like shape which starts releasing ligaments from its periphery. These leading-edge instabilities are recognized as Taylor instabilities whose occurrence depends on the strong enough deceleration forces [29]. At higher jet velocities, the relative flow parallel to the jet surface overcomes the surface tension effect and leads to stripping of droplets. These stripping from the jet surface can be of the form of Kelvin-Helmholtz instability (Figure 3.2(II)) which further causes the thinning of jet. At the Large relative velocity between the fluids results in small droplets and vice versa.

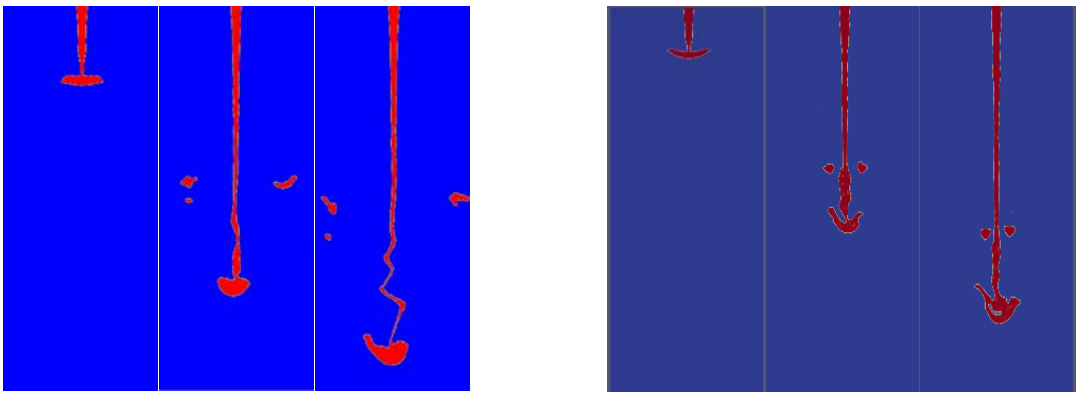

(a) (b)

I. $We_a = 1.25, D_j = 5\ mm, U_j = 0.5\ m/s$

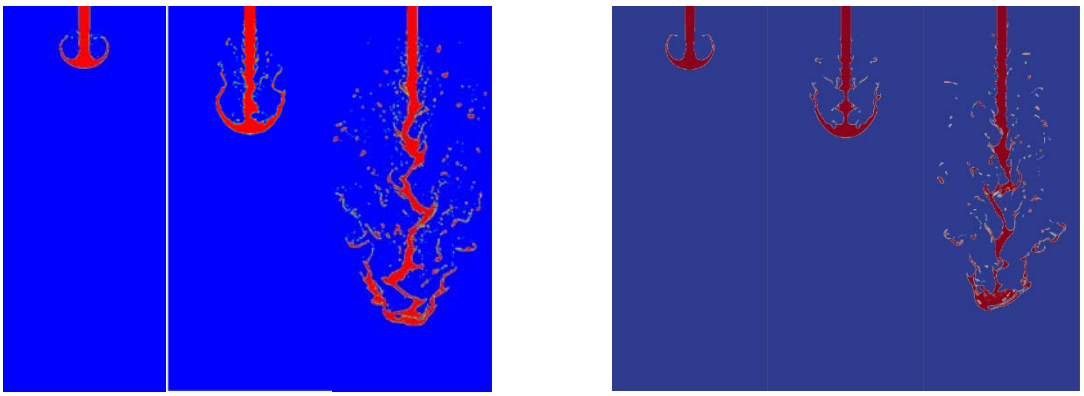

(a) (b)

II. $We_a = 125, D_j = 5\ mm, U_j = 5\ m/s$

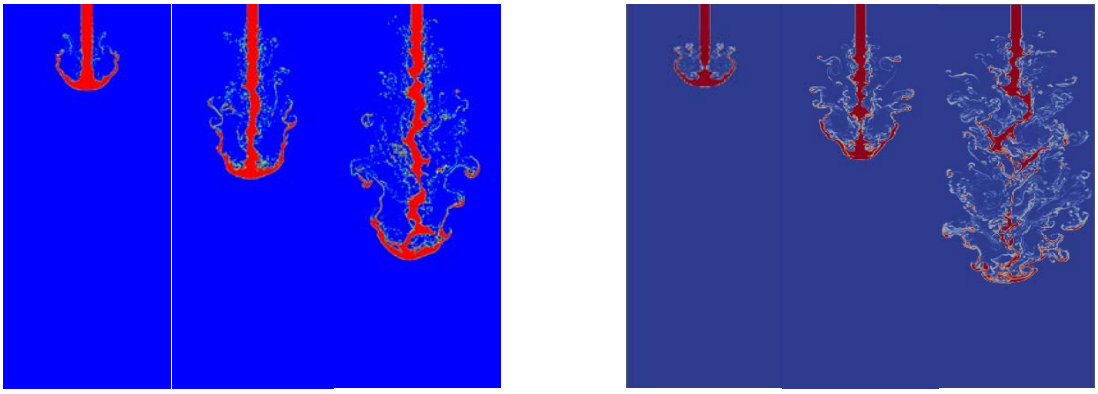

(a) (b)

III. $We_a = 1280, D_j = 5\ mm, U_j = 16\ m/s$

Fig. 3.2 Jet deformation and breakup while progression in a water pool.

(a) Thakre et al. [28] (b) present work

As the diameter of jet decreases due to the erosion from the surface, the jet column near the leading edge would break-up into large discrete "lumps" due to Rayleigh-Taylor's instability. Depending on the coolant volume and the jet Weber number, the breakup into droplets will continue until a stable size debris is formed. As shown in the Figure 3.2 (III) at the more higher jet injection velocity the jet breakup in the form of atomization regime where severe stripping occurs from the jet surface.

3.1.3 Jet Breakup Length

As the molten jet falls in the coolant the first instance when the cylindrical jet detached from its leading part, the process known as jet breakup and the its distance from the inlet point is called the jet breakup length. In the present analysis, a jet breakup length is taken as a length of a coherent jet similar to the terminology used in Thakre et al. [28]. A compression of jet breakup length has been down for the jet inlet velocity of 1.5 m/s with respect to jet breakup time with the Thakre et al. paper. Also, the effect of various parameters such as jet diameter, jet velocity, surface tension is taken in further study. The curve jet breakup length shows a definite trend for various breakup time step. Since the number of jet breakup (points) occurs in the Thakre paper more relative to the present work so the specific pattern of jet breakup is more visible. The variation in the jet breakup length between the two papers may happen due to the different mesh size or because of the choosing solution parameters. Within the given time step the

breakup length in the Thakre paper goes above 200 mm but it stays below 200 mm in the present simulation.

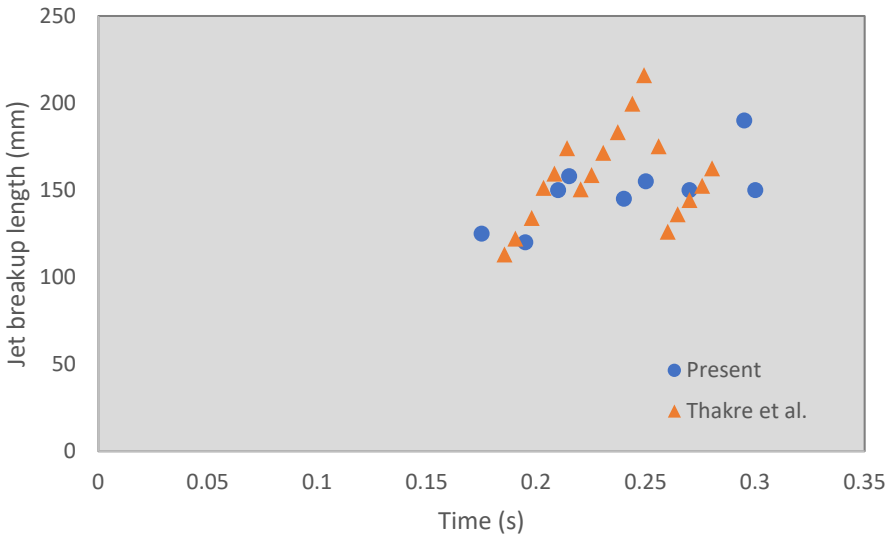

Fig. 3.3 Dynamics of the jet breakup where $D_j = 5\ mm$, $U_j = 1.5\ m/s$

3.1.4 Effect of Jet Diameter

The process of molten jet and coolant interaction is widely influence by the jet diameter. For the Significantly larger diameter of jet, Weber number (We_a) increases abruptly. which may appreciate atomization, i.e. the jet stripping from the surface increases. In order to understand the effect of jet diameter (D_j) on the jet breakup length (L), simulations with different jet diameter sizes have been carried out. Figure (3.4) shows the variation in jet breakup length with a size of melt jet and also a comparison between the present work and Thakre work, which shows that the breakup length increases as the diameter increases. The comparison is done for the jet diameter size of 5 mm, 7 mm and 10 mm.

3.1.5 Effect of Jet Velocity

A similar comparison is done here as shown in figure (1.2) given by Bürger et al. [22] and Ginsberg [21]. A curve has been plotted for the different value of Weber number i.e. at the wide range of inlet velocity with respect to dimensionless jet breakup length (represented by L/D). The present plot is showing a forward sift with respect to Thakre paer. Although the present simulation curve is more pronounced toward the Bürger et al. [22] plot shown in fig. (1.2).

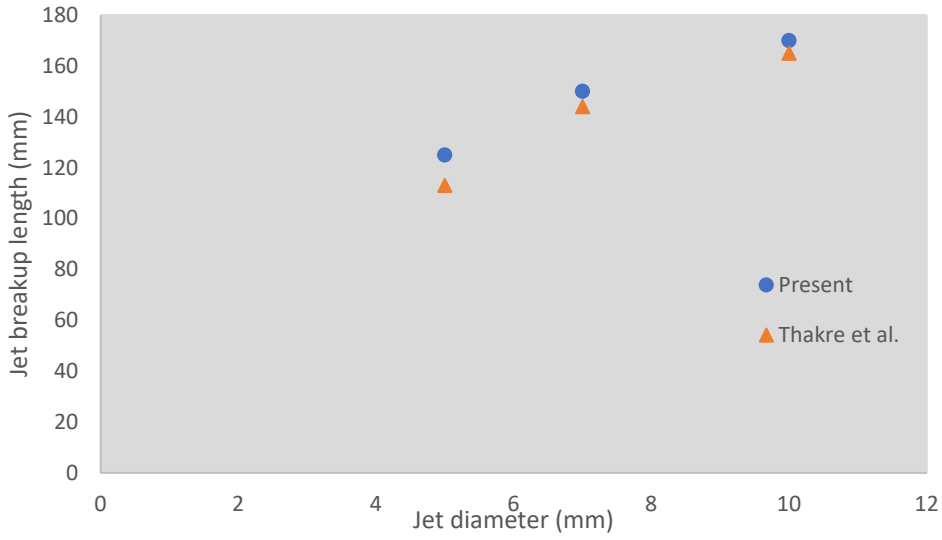

Fig. 3.4 Variation of jet breakup length with respect to jet diameter ($U_j = 1.5\ m/s$).

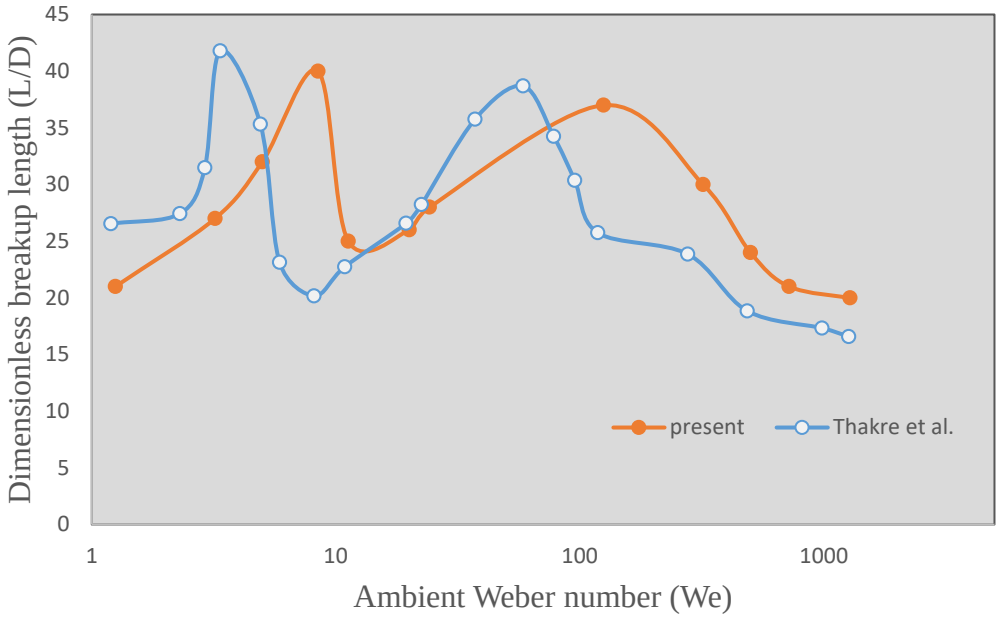

Fig 3.5 Variation of breakup length with respect to Weber number, ($D_j = 5\ mm$)

3.1.6 Effect of surface tension

According to the paper of Thakre et al. [28], for the smaller jets or jet droplets the effect of surface tension can be more dominant. At the lower surface tension, the jet surface is more capable of generating surface instabilities which further cause jet surface stripping and leads to thinning of the jet. As compare to higher value of surface tension these conditions may be responsible for an early breakup of jet where at higher

surface tension it can keep the jet surface intact. As discussed earlier in the text, the Rayleigh-Taylor type instability occurs to the jet in the normal direction near leading edge which causes the jet breakup and surface tension is one of the influencing factors in R-T instability theory. In case of linear theory, the minimum wavelength is given as $\lambda_c = \sqrt{\sigma_j / g(\rho_j - \rho_{s)}}$. this suggest that the surface tension may have some critical value deciding the critical wavelength for the jet of a specific melt-liquid density ratio [30]. A curve has been plotted with respect to different surface tension value as compared to Thakre paper.

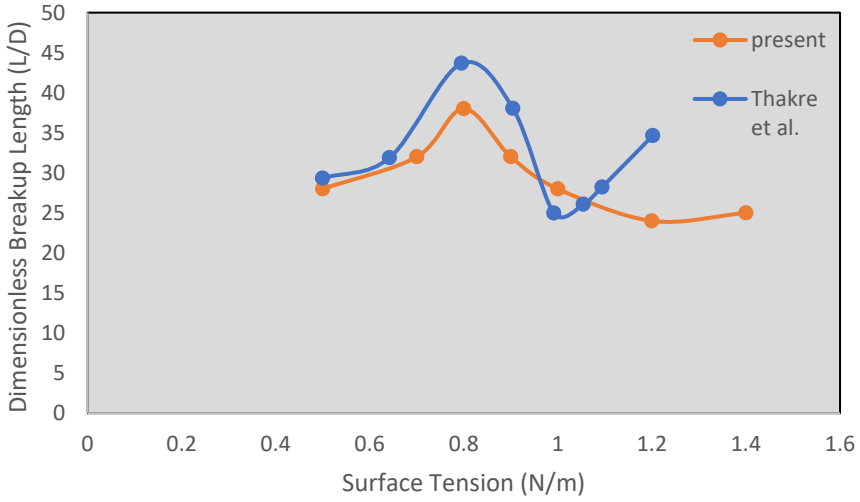

Fig 3.6 Effect of surface tension on jet breakup length ($D_j = 5\ mm$, $U_j = 1.5\ m/s$)

3.2 Droplet size distribution and sphericity

The size of the melt jet droplets (jet fragmented particles) has strong influence on the steam explosion. Hence the study of droplet size distribution is very important. For the calculation of the droplet size as well as sphericity MATLAB Image Processing Toolbox [30] is used. First, a visualization software, paraview is used to extract the images of the volume fraction distribution with a level of 0.5 to distinguish between the phases and mark the interface. MATLAB is used to convert the image into binary for it to identify the droplets as objects that have pixel value of 1, whereas the remaining portion having pixel value of 0 was identified as the water phase. Figure (2.1) shows the process of implementation of MATLAB image processing tool codes. The equivalent diameter (d) of the droplets was calculated from the simple relation of the diameter to the area of the droplets.

$$\text{Equivalent Diameter, } d = \sqrt{\frac{4A}{\pi}}$$

$$\text{Sphericity, } \quad S = \frac{P}{d},$$

Where, A = Area and P = Perimeter of a droplet

The form of droplet size distribution is shown in the fig. (3.7) with respect to different velocity and in fig. (3.8) with respect to diameter variation. Fig (3.7) shows that jet with lower velocity have less difference in size percentage and relatively wide range of variation. On the other hand, at the higher inlet jet velocity (10 m/s or more) higher number of fine droplets forms. For higher velocity jets, the relative flow parallel to the jet surface overcomes the surface tension effect and leads to stripping of droplets. These stripping from the jet surface can be of the form of Kelvin-Helmholtz instability, which further causes the thinning of jet. However, at lower jet velocities, the surface stripping is less and comparatively longer wavelength giving bigger size stripped droplets. Moreover, at lower velocities the leading-edge breakup is more dominant which results into bigger size droplets.

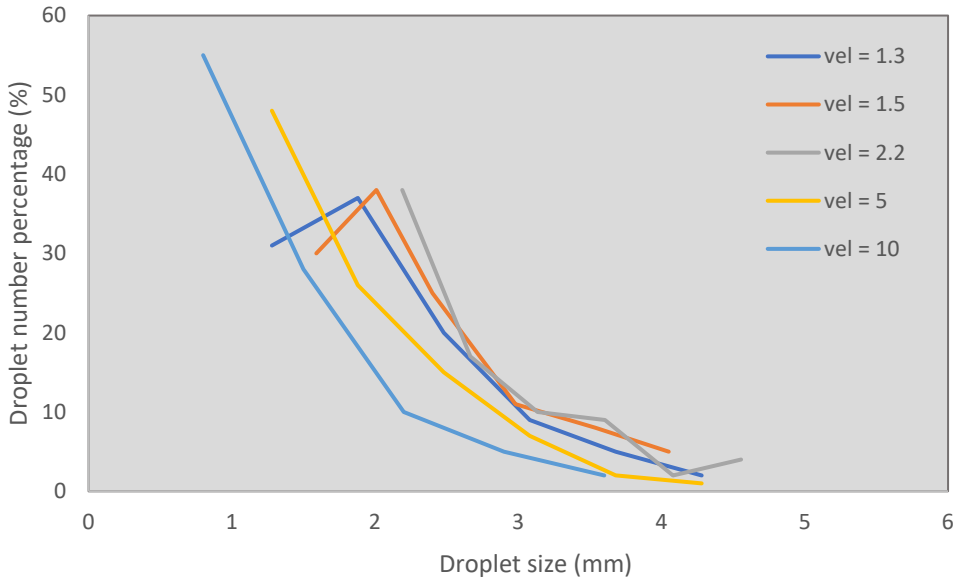

Fig. (3.7) droplet size distribution at different injection velocity ($D_j = 5\ mm$).

In the second comparison, fig. (3.8) three different diameter jets have been considered. The plot shows the droplet percentage with respect to their size at the injection velocity of 1.5 m/s. the result shows the range of droplet size between 1mm to 5mm (more

closely) and the curve takes the shape of exponentially decreasing (approximately), i.e. the percentage of droplets is maximum at the lower size. There is no significant effect of the diameter on the droplet size distribution found from these results.

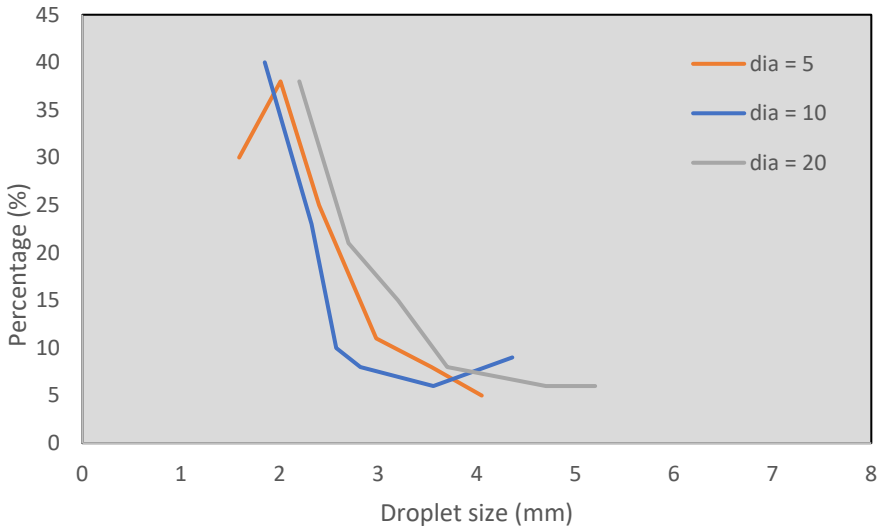

Fig. (3.8) Droplet size distribution for different diameter of jets ($U_j = 1.5\ m/s$)

The sphericity (S), which is a measure of the shape of the droplets, is calculated as the ratio of the equivalent diameter of the droplets to their perimeter. The toolbox includes an algorithm for determining the perimeter which gives more accurate values at higher number of pixels per object. The image processing algorithm includes cut-of limits as sphericity of 0.1 or more and area of 5000 pixels or less to identify an object as a droplet and to exclude the ligaments and the main jet in the calculations respectively. There are two curves have been plotted for the sphericity with respect to droplet number percentage.

From fig. (3.9) which is a plot for variation of sphericity at different velocity shown that, generally sphericity of droplet increases at some extent than decreases in the same manner. At the lower velocity sphericity variation is less more precisely varies between 2 to 6 mm and forms poisons like distribution. At higher velocity the sphericity is more spreaded and varies between 1 to 6 mm. also the number percentage of droplets is less at the higher velocity as compared to lower velocity. At lower velocities the sphericity shows a continuous increment which reaches the maximum and then decreases in the same manner. Whereas, at higher velocity curves shows different behaviour

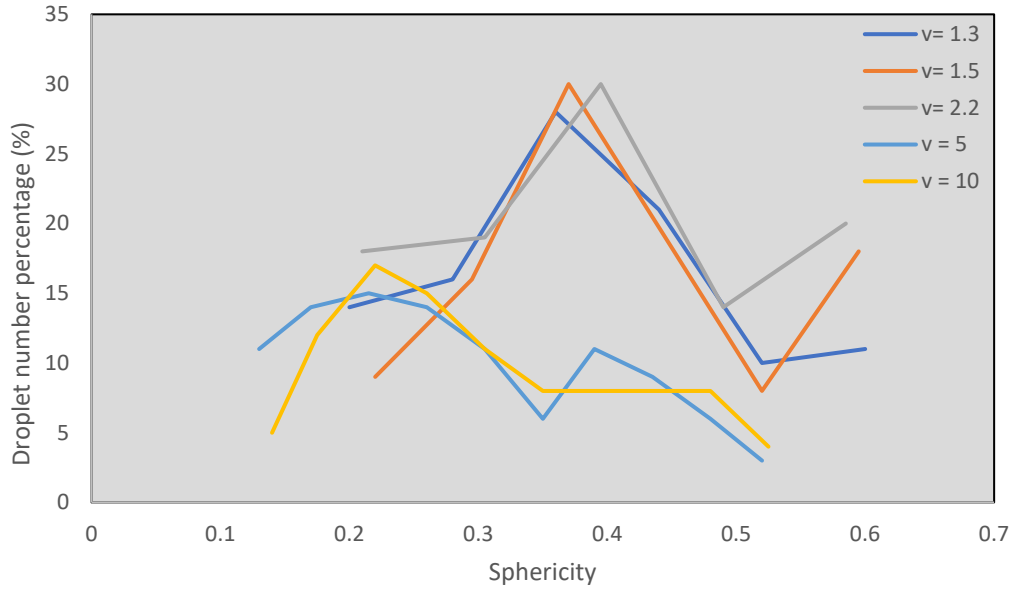

Fig. (3.9) Sphericity of jet droplets at different velocity ($D_j = 5\ mm$)

The variation of sphericity with respect to different diameter is shown in fig. (3.10). from the graph it is clear that the sphericity of the droplets for different diameter shows very similar pattern. The range of sphericity lies between 0.2 to 0.6 and at the higher inlet jet diameter the number percentage of lower spherical droplets is more.

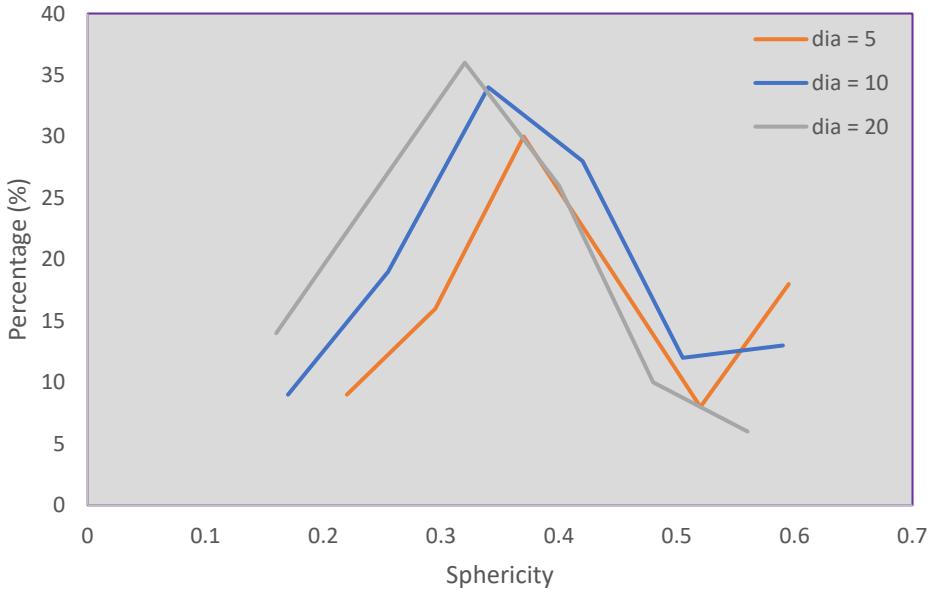

Fig. (3.10) Sphericity of the jet droplets at different diameter ($U_j = 1.5\ m/s$)

3.3 Simulations in presence of cylindrical channels

Present Simulations are motivated by the experimental investigation happened at the Jadavpur university in collaboration with BARC. In which cylindrical channels are taken at specific interval within the internal domain of tank. Which is a practical case of PHWR. Keeping the other transport properties (Table 2.1) and the boundary conditions the same, the geometry of the previous problem has increased to 320x320 mm. Due to the enormity of the number of computational channels, parallel simulations have been done with decomposing the domain geometry to get approximately equal number of channels in each decomposed domain. A HP work station with 4 GB RAM, Intel(R) Core(TM) i5-4200U CPU @ 2.30 GHz, is used for the numerical simulations.

3.3.1 Mesh quality

Relatively course mesh has been taken for the present work because of the larger simulation domain. To generate the mesh snappyHexMesh [31] utility (an advance meshing utility) is used here. Also, to create the cylindrical channels inside the domain an opensource software FreeCAD is used.

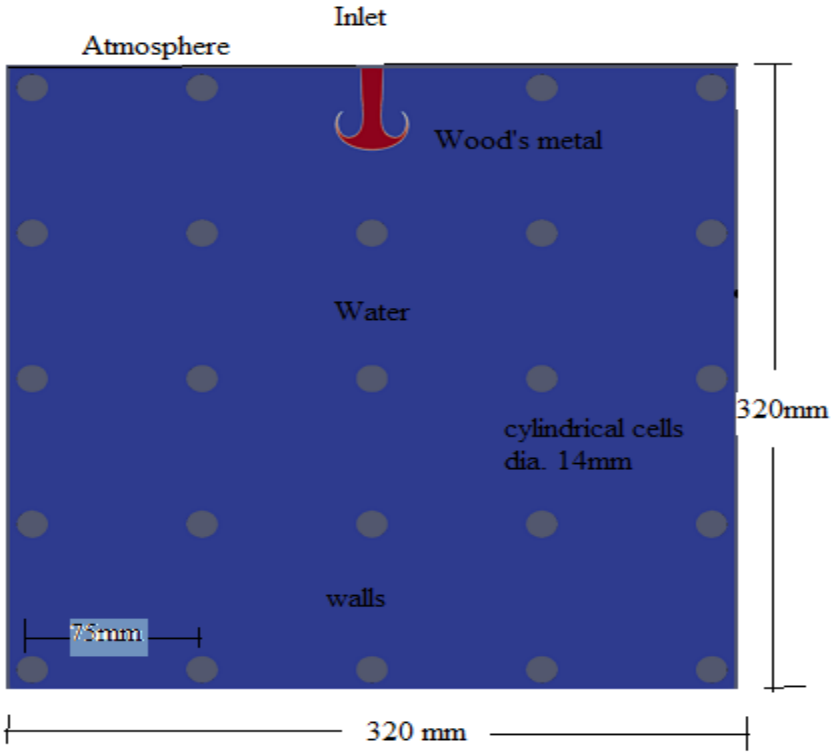

Fig. (3.11) Geometry details and boundary conditions.

Initially, using FreeCAD [32] part design tool box, cylindrical channels were generated at the particular locations in the domain as a stl file. Then in the meshing utility surfaceFeatureExtract and snappyHexMesh were used for generating eMesh file from stl file and to extrude, adding layer and patching the cylindrical channels as a wall respectively. Each of the cylindrical channels having the diameter of 14 mm and are at 75 mm from each other i.e. spacing between the cylindrical channels are 75 mm in horizontal as well as in the vertical directions.

3.3.2 Jet breakup pattern

Unlike the previous case (without cylindrical channels) where the jet breaks itself, in present simulation jet breaks after striking the cylindrical cell or channel. By shifting the cylindrical cell along the vertical axis, the breakup pattern may change. A compression of jet breakup pattern is being shown in the fig. (3.12) between the experimental setup at Jadavpur University and present hydrodynamic simulation. In the experimental setup molten metal has superheat temperature of 30 degree Celsius and the other conditions were the same as taking simulation.

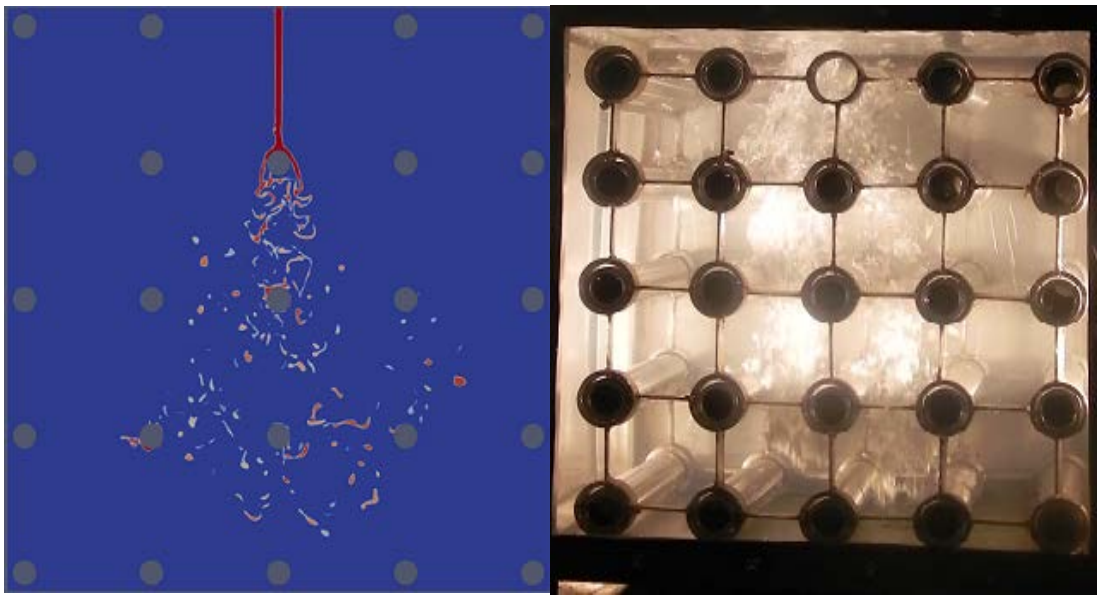

(a) (b)

Fig. 3.12 (a) An isothermal jet breakup pattern at Dj=5 mm, Uj=2 m/s (b) an experimental setup and jet breakup at JU

3.3.3 Effect of jet velocity and diameter

Since jet breaks after sticking the cylindrical cell, there is no significance of jet inlet velocity and jet diameter on the jet breakup length. From injection to strike the

cylindrical cell jet travels as an intact jet form. The variation in the breakup mechanism of after striking the channels may depends on the inlet velocity and the jet injection diameter. Simulations for the different value of jet injection diameter has been carried out. Fig 3.13 (a) is shown with the jet inlet diameter of 5 mm at the time step of 0.2 second. At the same time step the break pattern has been shown in the fig. 3.13 (b) for the inlet diameter of 10 mm and 20 mm at the inlet velocity of 2 m/s.

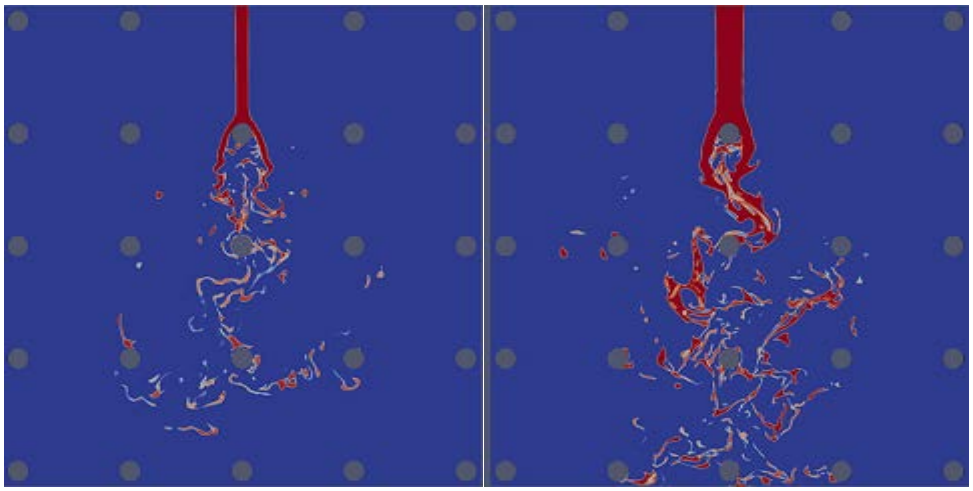

(a) (b)

Fig. 3.13 (a) at $D_j = 10\ mm$, $U_j = 2\ m/s$, (b) at $D_j = 20\ mm$, $U_j = 2\ m/s$

3.3.4 Droplet size distribution and sphericity

The calculation procedure for finding the droplet size distribution and the sphericity is similar to the previous case. For the different inlet jet diameter, two plots

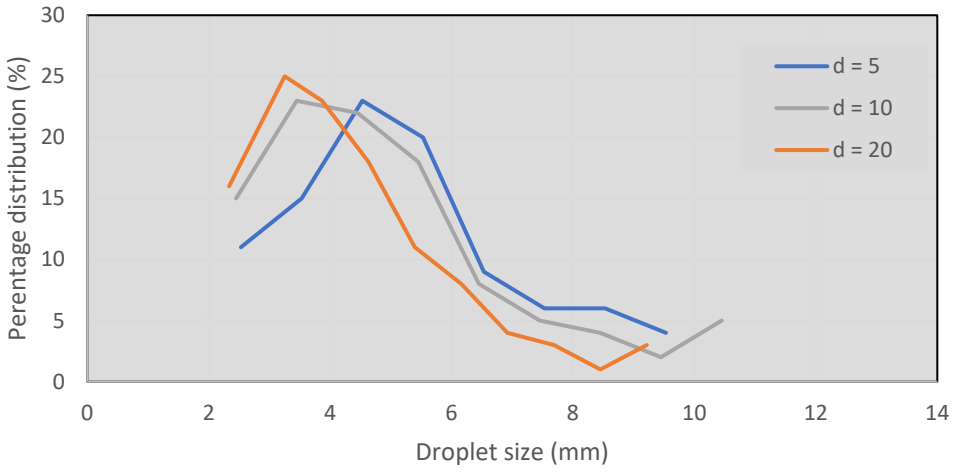

Fig. 3.14 Droplet size distribution at different Diameter. ($U_j = 2\ m/s$)

have been shown to compare the droplet size distribution and the sphericity. The size distribution of droplets shows more wider variation (2mm to 11mm) with respect to the previous case (without cylindrical channels). The variation in Sphericity of the droplets are similar to the previous case i.e. in the case of jet fragmentation without cylindrical channels. The range of sphericity is between 0.1 to 0.7 which shows more spread behaviour related to the simulation of without cylindrical channels. For each simulation cases of inlet jet diameter, sphericity reaches the maximum between 0.2 to 0.4 values then decreases in the same manner.

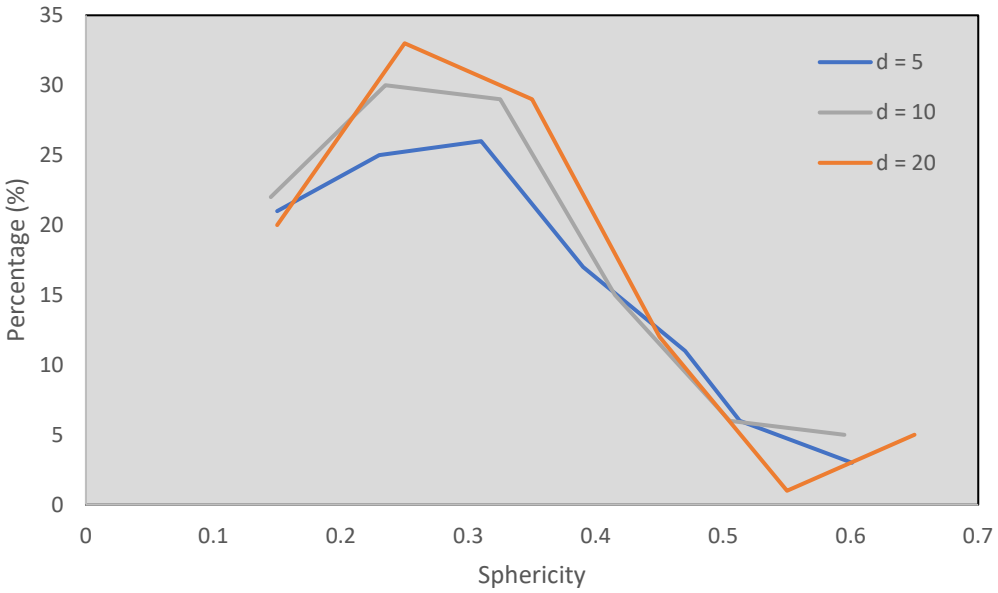

Fig. 3.15 Sphericity of droplets at different diameter ($U_j = 2\ m/s$).

CHAPTER 4

CONCLUSIONS

A two-dimensional numerical analysis of melt jet breakup phenomenon has been carried out using InterFoam (VOF based algorithm) solver. For simulation purposes, an opensource CFD code, OpenFOAM 6.0 and for droplet size distribution MATLAB 2014b have been used. The study includes the jet fragmentation behaviour as well as the influences of jet diameter, jet velocity and physical property like surface tension on the jet breakup length. The simulation of multiphase flow using InterFoam is highly depends on mesh size to capture distinct interface between different phases. Also, the dynamics of jet breakup pattern highly depends on Weber number. The salient conclusions which are drawn from the simulation results are summarised in the following-

1. Jet breakup pattern shows a mushroom like shape or an axisymmetric behaviour during the initial deformation of jet and shape disturbs as the instability grows.
2. At the lower jet velocity, leading edge breakup is found to be dominant. However, the sideways stripping effect increases as jet velocity is increased.
3. The overall behaviour of the jet breakup shows good agreement with the work of Thakre et al. It is found that the jet breakup length increases with the increase in inlet jet diameter. The dimensionless jet breakup length shows quite good agreement with the work of Bürger et al. for different jet injection velocities.
4. Droplet size distribution analysis shows there is no significant effect of jet diameter on the size distribution of the droplets. However, observation (Fig. 3.7) reveals that at higher jet injection velocity the percentage of fine size droplets increases.
5. There is no any significance of different jet diameter on sphericity of the fragmented jet droplets. But at higher velocity the sphericity range increases and lowering the droplet percentage. The curve somewhat follows the Poisson's like distribution.
6. For the simulation of jet breakup in presence of cylindrical channels, it is observed that there is no effect of inlet jet diameter on the jet breakup length. The shape of the curve of droplet size distribution as well as sphericity with

droplet number percentage found to be more similar with the cases where no cylindrical channel is present. However, the range of the droplet size increases in presence of channels. In addition, results also shows that the sphericity curve follows Poisson’s like distribution.

REFERENCES

[1] S. Thakre, Weimin Ma, Liangxing Li; A numerical analysis on hydrodynamic deformation of molten droplets in a water pool, Annals of Nuclear Energy 53 (2013) 228-237.

[2] T.G. Theofanous; The study of steam explosions in nuclear systems, Nuclear Engineering and Design (1995).

[3] D.F. Fletcher and R.P. Anderson; A review of pressure-induced propagation models of the vapour explosion process, Progress in Nuclear Energy vol. 23, No. 2 1990

[4] Ryusuke Saitoa, Yutaka Abea and Hiroyuki Yoshidab; Experimental study on breakup and fragmentation behaviour of molten material jet in complicated structure of BWR lower plenum, Journal of Nuclear Science and Technology, 2014 Vol. 51, No. 1, 64–76.

[5] Meister B. J. and Scheele G. F., Prediction of jet length in immiscible liquid systems, AICHE J. 1969; 15: 689-699

[6] Tomotika, On the instability of a cylindrical thread of a viscous liquid surrounded by another viscous fluid, Proceedings of Royal Society A 1935; 150: 322–337

[7] Meister, B. J., Scheele, G. F., Prediction of jet length in immiscible liquid systems, AICHE J. 1969; 15: 689- 699

[8] Lee, W. K. and Flumerfelt, R. W., Instability of stationary and uniformly moving cylindrical fluid bodies-I. Newtonian systems, Int. J. Multiphase Flow 1981; 7: 363-383.

[9] Kinoshita, C. M., Teng, H., Masutani, S. M., A study of the instability of liquid jets and comparison with Tomotika's analysis. Int. J. Multiphase Flow 1994; 20: 523-533.

[10] Chacha, M., Radev, S., Tadrist, L., and Occelli, R., Numerical treatment of the instability and the breakup of a liquid capillary column in a bounded immiscible phase, Int. J. Multiphase Flow 1997; 23: 377-395

[11] Kitamura, Y., Michima, H. and Takahashi, T., Stability of jets in liquid-liquid systems. Can. J. Chemical Engineering 1982; 60: 723-731

[12] Saito, M. et al., Experimental study on penetration behaviours of water jet into freon-11 and liquid nitrogen. ANS Proceedings of National Heat transfer Conference, Houston, Texas, 1988

[13] S.P. Lin, R.D. Reitz, Drop and spray formation from a liquid jet, Annual Re- views Fluid Mechanics, 30 (1998) 85-105.

[14] R.D. Reitz, Modeling primary atomization processes in high-pressure vaporizing sprays, Atomization and Spray Technology 3:4 (1987) 309-337.

[15] V. Ariane, A.A. Burluka, R. Borghi, Development of a Eulerian model for the ‘‘atomization’’ of a liquid jet, Atomization and Sprays, 11 (2001) 619-642.

[16] A.A. Ibrahim, M.A. Jog, Nonlinear breakup model for a liquid sheet emanating from a pressure-swirl atomizer, Journal of Engineering for Gas Turbine and Power, 129 (2007) 945-953.

[17] Theofanous, T. G., Saito, M., An assessment of Class-9 (Core-Melt) Accidents for PWR Dry-Containment Systems. Nuclear Engineering and Design, 1982; 66: 307- 332.
[18] Epstein, M., Fauske, H. K., Steam film instability and the mixing of core-melt jets and water. ANS Proceedings of the National Heat Transfer Conference, Denver, Colorado, USA 1985, 277–284
[19] Schins, H., Gunnerson, F. S., Boiling and fragmentation behavior during fuel sodium interactions, Nuclear Engineering and Design 1986; 91: 221-235
[20] Yutaka Abea, Eiji Matsuo, Takahiro Arai, Hideki Nariai, Keiko Chitose, Kazuya Koyamac, Kazuhiro Itoh; Fragmentation behaviour during molten material and coolant interactions, Nuclear Engineering and Design 236 (2006) 1668–1681
[21] Ginsberg, T., "Liquid jet breakup characterization with application to melt water mixing," ANS Proc. National Heat Transfer Conf., Denver, CO. (1985).
[22] Bürger, M., Cho, S.H., Berg, E. V., Schatz, A., "Breakup of melt jets as pre-condition for premixing: Modelling and experimental verification," Nuclear engineering and design, Vol. 155, pp. 215-251 (1995).
[23] OpenFOAM user guide and tutorials, https://www.openfoam.com/documentation/user-guide/
[24] H. Jasak, A. Jemcov, Z. Tukovic, OpenFOAM: A C++ library for complex physics simulations, International workshop on coupled methods in numerical dynamics, 1000 (2007) 1-20.
[25] OpenFOAM user guide and tutorials, https://www.openfoam.com/documentation/user-guide/
[26] C.W. Hirt, B.D. Nichols, Volume of fluid (VOF) method for the dynamics of free boundaries, Journal of Computational Physics, 39:1 (1981) 201-225.
[27] J.U. Brackbill, D.B. Kothe, C. Zemach, A Continuum Method for Modelling Surface Tension, Journal of Computational Physics, 100 (1992) 335-354.
[28] S. Thakre, Louis Manickam, Weimin Ma; A numerical simulation of jet breakup in melt coolant interactions, Annals of Nuclear Energy 80 (2015) 467-475.
[29] Bürger, M., Cho, S.H., Berg, E. V., Schatz, A., "Breakup of melt jets as precondition for premixing: Modelling and experimental verification," Nuclear engineering and design, Vol. 155, pp. 215-251 (1995).
[30] Sharp, D. H., "An overview of Rayleigh-Taylor instability," Physical Nonlinear Phenomena, Vol. 12(1), pp. 3-18 (1984).
[31] MATLAB and Image Processing Toolbox, Release R2014a.
[32] FreeCAD part design user guide and tutorial.

APPENDIX I

MATLAB IMAGE PROCESSING CODE

```
%% read
scale = 0.5;
I = imread('imagename.png');
Igray = rgb2gray(I);
imshow(Igray)
%% binary black and white
level = 0.5;
BW = im2bw(Igray, level);
STATS = regionprops(BW, 'all');
figure(1);imshow(BW);hold on;
filename=sprintf('Binary Image.jpg');
saveas(gcf,filename);
hold off
[B, ~, N]=bwboundaries(BW);                    %first N channels in B represent
object boundaries
Dia=zeros(N,1);
P=zeros(N,1);
A=zeros(N,1);
K=zeros(N,1);

for i=1:N
   A(i,1)=STATS(i).Area;                       %Area of each object
   Dia(i,1)=STATS(i).EquivDiameter;            %Equivalent
Diameter(=sqrt(4*A/pi)) of each object
   P(i,1)=STATS(i).Perimeter;                  %Perimeter of each object
end
```

```
for i=1:N
   Sphericity=Dia(i,1)/P(i,1);
   K(i,1)=Sphericity;                                %Trial sphericity of each object
end
DiaTrue=Dia*scale;
 r=1;
for i=1:N
   if A(i,1)>=3 && A(i,1)<=50000
      if K(i,1)>=0.1
      Diameter(r,1)=DiaTrue(i,1);
      SphericityTrue(r,1)=K(i,1);
      r=r+1;
      end
   end
end

Histogram=Diameter;
xlswrite('Diameter.xlsx',Histogram);          % rows=droplets diameters

Histogram1=SphericityTrue;
xlswrite('Sphericityd.xlsx',Histogram1);       % rows=droplets diameters
```

APPENDIX II

surfaceFeatureExtract file

```
FoamFile
{
    version     2.0;
    format      ascii;
    class       dictionary;
    object      surfaceFeatureExtractDict;
}
// * * * * * * * * * * * * * * * * * * * * * * * * * * * * * * * * * * * * * * * * //

cylinder.stl
{
    extractionMethod    extractFromSurface;
    includedAngle       180;
    subsetFeatures
    {
        nonManifoldEdges       no;
        openEdges       yes;
    }
    writeObj            yes;
}
//
**********************************************************************
**** //
```

SnappyHexMesh file

```
FoamFile
{
   version     2.0;
   format      ascii;
   class       dictionary;
   object      snappyHexMeshDict;
}
// * * * * * * * * * * * * * * * * * * * * * * * * * * * * * * * * * * * * * * * * //

// Which of the steps to run
castellatedMesh true;
snap            true;
addLayers       true;
geometry
{
   cylinder.stl                    // stl file created by FreeCad software
   {
      type triSurfaceMesh;
      name cylinder;
   }
   refinementBox
   {
      type searchableBox;                  // must include the whole mesh domain
      min (-0.01 -0.01 -0.01);
      max ( 0.33  .0012 .52);
   }
};
castellatedMeshControls
```

```
{
    // Refinement parameters
    // ~~~~~~~~~~~~~~~~~~~~~~

    maxLocalChannels 100000;
    maxGlobalChannels 200000;
    minRefinementChannels 10;
    maxLoadUnbalance 0.10;
    nChannelsBetweenLevels 3;
    // Explicit feature edge refinement
    // ~~~~~~~~~~~~~~~~~~~~~~~~~~~~~~~~

    features
    (
        {
            file "cylinder.eMesh";              // generated by surfaceFeatureExtract
            level 2;
        }
    );
    // Surface based refinement
    // ~~~~~~~~~~~~~~~~~~~~~~~~

    refinementSurfaces
    {
        cylinder
        {
            // Surface-wise min and max refinement level
            level (1 1);
            {
                type wall;
```

```
            inGroups (cylinderGroup);
        }
    }
}

// Resolve sharp angles
resolveFeatureAngle 30;
// Region-wise refinement
// ~~~~~~~~~~~~~~~~~~~~~~~~

refinementRegions
{
    refinementBox
    {
        mode inside;
        levels ((1E15 3));
    }
}
// Mesh selection
// ~~~~~~~~~~~~~~~

locationInMesh (0.16 .0005 0.319);  // point must lies in the domain except cylinder
allowFreeStandingZoneFaces true;
}
// Settings for the snapping.
snapControls
{
nSmoothPatch 3;
tolerance 2.0;
nSolveIter 30;
```

```
    nRelaxIter 5;

    // Feature snapping
        nFeatureSnapIter 10;
        implicitFeatureSnap false;
        explicitFeatureSnap true;
        multiRegionFeatureSnap false;
}
// Settings for the layer addition.
addLayersControls
{
    relativeSizes true;
    layers
    {
        "(cylinder).*"
        {
            nSurfaceLayers 3;
        }
    }
    // Expansion factor for layer mesh
    expansionRatio 1.0;
    finalLayerThickness 0.3;
    minThickness 0.1;
    nGrow 0;
    featureAngle 60;
    slipFeatureAngle 30;
    nRelaxIter 3;


    nSmoothSurfaceNormals 1;
```

```
    nSmoothNormals 3;
    nSmoothThickness 10;
    maxFaceThicknessRatio 0.5;
    maxThicknessToMedialRatio 0.3;
    minMedianAxisAngle 90;
    nBufferChannelsNoExtrude 0;
    nLayerIter 50;
}
meshQualityControls
{
    #include "meshQualityDict"
    nSmoothScale 4;
    errorReduction 0.75;
}
mergeTolerance 1e-6;
//
*********************************************************************
**** //
```